ACTIVE WHIRL FLUTTER SUPPRESSION USING CONTROL SURFACES

Bedirhan Yilmaz
Istanbul Technical University
Turkish Aerospace Industries
Istanbul, TR

Aykut Tamer
University of Bath
Bath, UK

Ali Tatar
Istanbul Technical University
Istanbul, TR

ABSTRACT

Whirl flutter is a stability problem caused by the interaction between aerodynamic, inertial, elastic forces, and gyroscopic effects from rotating propellers or rotor blades. Detailed analyses and flight tests are conducted to ensure stability; however, additional flutter control measures can be implemented to enhance stability further. For this purpose, active control strategies offer adaptive and effective solutions, dynamically adjusting to real-time flight conditions. This study presents an active control application designed to enhance the critical whirl flutter speed of an aircraft by utilizing existing primary control surfaces, eliminating the need for additional actuators or surfaces. To demonstrate this approach, a numerical simulation is performed using a 6-DoF dynamics of a model aircraft, modified by incorporating a twin prop-rotor engine, formulated using Reed's model equations. Then, a PID-based active control system is implemented, which utilizes angular rate feedback from the proprotor thrust system to generate control commands for the ailerons and rudder. Numerical simulation results show that this approach can successfully increase the aircraft's critical whirl flutter speed by 14.6%

NOTATION

*

Symbols

a Distance between propeller hub and center of gravity, m

A_1, A_2, A_3 Aerodynamic coefficients of propeller

c_b Chord length of propeller blades, m

cl_α Lift slope of propeller blades, rad^{-1}

C_θ, C_ψ Structural damping of proprotor support, Nm s rad^{-1}

$\mathbf{F}_{AC}$ Force acting on the aircraft, N

$\mathbf{F}_{Aero}$ Aerodynamic forces, N

$\mathbf{F}_{Eng}$ Propulsive forces, N

$\mathbf{F}_{Hub}$ Force acting ın the propeller hub, N

$\mathbf{F}_{Mass}$ Inertial forces, N

$\mathbf{I}$ Moment of inertia of the aircraft, kg·m^2

I_r Moment of inertia of the rotor, kg·m^2

I_n Moment of inertia of the nacelle, kg·m^2

K_a Aerodynamic coefficient of propeller

K_p, K_i, K_d Proportional, integral, and derivative gains of the PID controller

K_θ, K_ψ Structural stiffness of proprotor support, Nm rad^{-1}

m Mass of the aircraft, kg

m_p Mass of the proprotor system, kg

$\mathbf{M}_{AC}$ Moment acting on the aircraft, Nm

$\mathbf{M}_{Aero}$ Aerodynamic moments, N·m

$\mathbf{M}_{Eng}$ Propulsive moments, Nm

$\mathbf{M}_{Hub}$ Moments acting on the propeller hub, Nm

$\mathbf{M}_{Mass}$ Inertial moments, Nm

N_b Number of propeller blades

p, q, r Angular velocity components of the aircraft, rad/s

R Rotor radius, m

$\ddot{\mathbf{r}}$ Linear acceleration of the aircraft, m/s^2

q_p, r_p angular velocity components of proprotor system, rad/s

T_0 Initial propeller thrust force, N

V Velocity vector of the aircraft, m/s

u, v, w Velocity vector components, m/s

α Angle of attack, rad

β Sideslip angle, rad

$\delta_{Aileron,Cmd}, \delta_{Rudder,Cmd}$ Control surface deflection of aileron and rudder

$\Delta x, \Delta y, \Delta z$ Distance between proprotor cg and aircraft cg, m

μ Propeller advance ratio

ρ Air density, kg/m^3

ϕ, θ, ψ Euler angles (roll, pitch, yaw), rad

θ^* Effective pitch angle, rad

ψ^* Effective yaw angle, rad

$\boldsymbol{\Omega}$ Angular velocity of propellers, rad/s

$\boldsymbol{\omega}$ Angular velocity of the aircraft, rad/s

*

Acronyms

DoF Degree of Freedom

PID Proportional-Integral-Derivative

AC Aircraft center of gravity point

cg Center of Gravity

INTRODUCTION

After investigations conducted by (Ref. 1) revealed that two accidents involving the Lockheed L-188 Electra since the 1960s were caused by an aeroelastic instability known as whirl flutter, it has become crucial to include the loads generated by rotating propellers and their interaction with elastic supports in the flutter analysis of proprotor aircraft. This instability arises from the interaction between the aerodynamic, inertial and elastic forces generated by the aircraft's propellers or rotor blades and the gyroscopic forces due to their rotation. Such interactions can greatly impact the stability and safety of the aircraft, potentially leading to dangerous conditions if not properly controlled. As high-speed aircraft and rotorcraft continue to evolve, especially considering the new generation of propeller-driven aircraft such as tilt-rotor turboprops and vertical take-off and landing (VTOL), understanding and mitigating whirl flutter has become increasingly essential to ensure their reliable and safe operations.

Historically, Reed's model (Ref. 2) has been the cornerstone for predicting whirl flutter stability in propellers, which was introduced in the mid-20th century and reformulated by Bielawa (Ref. 3). This model provided a minimum complexity framework for analyzing the dynamic interactions that lead to whirl flutter. Known as the two degrees of freedom whirl flutter model, it considers both pitching and yawing motions along with the associated gyroscopic and aerodynamic moments. This model has been extensively validated through both linear and nonlinear analyses across various configurations in (Refs. 4–6). The application of this model has led to significant advancements for understanding the whirl-flutter phenomenon. Researchers have extended this model in (Ref. 7) to analyze the stability boundaries of different rotorcraft and aircraft configurations, contributing to the development of safer and more stable designs. For instance, comprehensive studies have shown in (Refs. 8, 9) how varying rotor speeds, blade stiffness, and other aerodynamic parameters influence the onset of whirl flutter. These insights have been critical in the design stages of modern aircraft, where optimizing stability margins against whirl flutter is a key consideration. However, there are cases where these structural improvements may not be sufficient, or they may be impractical due to weight, cost, or design constraints. In such cases, the focus shifts to control strategies—either passive or active—to suppress whirl flutter.

The stability of tiltrotor aircraft can be effectively enhanced by designing wing extensions and winglets in (Ref. 10), utilizing the piezoelectric effect in (Ref. 11), or manipulating the composition of composite materials in (Refs. 12–14) to modify the stiffness of the wing and rotor, thereby influencing their aeroelastic behaviour. By carefully optimizing these factors, it is possible to improve tiltrotor stability across the entire operational envelope, even without relying on active control systems. However, despite the effectiveness of these passive methods, they are often constrained by specific design and aerodynamic conditions of the aircraft. For instance, adding winglets or extensions may introduce additional drag or structural complications, limiting their effectiveness under certain flight conditions.

Due to the limitations of passive control methods, there has been a growing need for more flexible and adaptable solutions, leading to increased interest in active control approaches for whirl flutter suppression. Unlike passive control methods, active control methods can adjust in real time to varying flight conditions, providing greater flexibility and effectiveness. These systems have shown distinct advantages in mitigating vibrations and enhancing aeroelastic stability, particularly in high-performance aircraft where speed and maneuverability are critical. By integrating advanced modelling techniques with innovative control strategies, the aerospace industry can develop safer, more efficient, and more reliable aircraft, capable of operating under increasingly demanding conditions.

Among the various active control strategies, the usage of rotor swash-plates has been a practical approach, frequently studied and implemented by (Refs. 15, 16) in the past. These systems allow for precise control of rotor blade pitch, enabling the aircraft to maintain stability even in the presence of destabilizing forces. Building on this, (Refs. 17–19) have developed active control system designs that increase whirl flutter speed and damping by using flaperon and aileron control surfaces. These studies have demonstrated the potential usage of active control systems to suppress whirl flutter by dynamically adjusting control surfaces in response to aerodynamic forces.

Whirl flutter involves an elliptical precessional motion with both vertical and horizontal components in the aircraft rotor, typically controlled across both axes using a swashplate. However, when control surfaces such as ailerons or flaperons are used, most inputs primarily affect only one axis. It is expected that generating control commands for both axes within the system will improve overall performance compared to systems addressing a single axis. Consequently, an active control system that generates both rudder and aileron inputs is expected to perform more effectively. Building on these insights, the main aim of this paper is to show that the usage of primary control surfaces, such as the rudder and aileron, in an active control system could offer a promising approach to suppressing whirl flutter while enhancing the stability and performance of high-speed aircraft. This approach also provides an opportunity to observe the results of active whirl flutter suppression on a full-span aircraft model, unlike previous studies that focused on semi-span models.

This paper begins with a brief review of the 6-DoF aircraft model. Following this, Reed's classical whirl flutter model is introduced and integrated with the aircraft's rigid-body equations of motion to examine and suppress whirl flutter. The subsequent section provides an overview of the control system design. Finally, the results of the numerical simulations are presented and discussed, highlighting the impact of the developed active control system.

METHODOLOGY

Aircraft Equation of Motion

The total forces and moments acting on the aircraft with two engines are as follows,

$$\mathbf{F}_{AC} = \mathbf{F}_{Mass} + \mathbf{F}_{Aero} + \mathbf{F}_{Eng(1,2)} \tag{1}$$
$$\mathbf{M}_{AC} = \mathbf{M}_{Mass} + \mathbf{M}_{Aero} + \mathbf{M}_{Eng(1,2)} \tag{2}$$

A 6-DoF aircraft model represents the motion of an aircraft in three-dimensional space. In the body-fixed coordinate system, the translational equations of motion are:

$$m \cdot \ddot{\mathbf{r}} + m \cdot (\boldsymbol{\omega} \times \mathbf{V}) = \mathbf{F}_{AC} \tag{3}$$

And the rotational motion of the aircraft is governed by Euler's equations of motion in the body-fixed coordinate system,

$$\mathbf{I}\dot{\boldsymbol{\omega}} + \boldsymbol{\omega} \times (\mathbf{I}\boldsymbol{\omega}) = \mathbf{M}_{AC} \tag{4}$$

Engine (Proprotor) Model

Reed's classical whirl flutter model, when used in the context of the simplicity of the quasi-steady assumption, was reformulated by Bielawa (Ref. 3) to account for the disturbing forces and moments at the rotor hub generated by propellers. If we rewrite these equations by incorporating the effects of the aircraft's orientation using the effective angles (α and β),

$$I_n\ddot{\theta}^* - I_x\Omega\dot{\psi}^* + C_\theta\dot{\theta} + K_\theta\theta = -M_{y,Hub} + aRF_{z,Hub} \tag{5}$$
$$I_n\ddot{\psi}^* + I_x\Omega\dot{\theta}^* + C_\psi\dot{\psi} + K_\psi\psi = M_{z,Hub} + aRF_{y,Hub} \tag{6}$$
$$\theta^* = \theta + \alpha \tag{7}$$
$$\psi^* = \psi + \beta \tag{8}$$
$$\dot{\theta}^* = \dot{\theta} + \dot{\alpha} \tag{9}$$
$$\dot{\psi}^* = \dot{\psi} + \dot{\beta} \tag{10}$$

Aerodynamic forces and moments at the propeller hub point, are;

$$F_{y,Hub} = \frac{\partial F_{y,Hub}}{\partial \psi}\psi^* + \frac{\partial F_{y,Hub}}{\partial \dot{\psi}}\dot{\psi}^* + \frac{\partial F_{y,Hub}}{\partial \dot{\theta}}\dot{\theta}^* = \frac{N_b}{2}K_a\left(A_1'\psi^* - aA_1\frac{\dot{\psi}^*}{\Omega} + A_2\frac{\dot{\theta}^*}{\Omega}\right) \tag{11}$$

$$F_{z,Hub} = \frac{\partial F_{z,Hub}}{\partial \theta}\theta^* + \frac{\partial F_{z,Hub}}{\partial \dot{\theta}}\dot{\theta}^* + \frac{\partial F_{z,Hub}}{\partial \dot{\psi}}\dot{\psi}^* = \frac{N_b}{2}K_a\left(A_1'\theta^* - aA_1\frac{\dot{\theta}^*}{\Omega} - A_2\frac{\dot{\psi}^*}{\Omega}\right) \tag{12}$$

$$M_{y,Hub} = \frac{\partial M_{y,Hub}}{\partial \psi}\psi^* + \frac{\partial M_{y,Hub}}{\partial \dot{\psi}}\dot{\psi}^* + \frac{\partial M_{y,Hub}}{\partial \dot{\theta}}\dot{\theta}^* = \frac{N_b}{2}K_aR\left(A_2'\psi^* - aA_2\frac{\dot{\psi}^*}{\Omega} + A_3\frac{\dot{\theta}^*}{\Omega}\right) \tag{13}$$

$$M_{z,Hub} = \frac{\partial M_{z,Hub}}{\partial \theta}\theta^* + \frac{\partial M_{z,Hub}}{\partial \dot{\theta}}\dot{\theta}^* + \frac{\partial M_{z,Hub}}{\partial \dot{\psi}}\dot{\psi}^* = \frac{N_b}{2}K_aR\left(A_2'\theta^* - aA_2\frac{\dot{\theta}^*}{\Omega} - A_3\frac{\dot{\psi}^*}{\Omega}\right) \tag{14}$$

$$K_a = \frac{1}{2}\rho c_{l\alpha}R^4\Omega^2 \tag{15}$$
$$A_1 = \int_0^1 \frac{c}{R}\frac{(\mu/\pi)^2}{\sqrt{(\mu/\pi)^2+\eta^2}}\,d\eta; \quad A_1' = (\mu/\pi)A_1 \tag{16}$$
$$A_2 = \int_0^1 \frac{c}{R}\frac{(\mu/\pi)\eta^2}{\sqrt{(\mu/\pi)^2+\eta^2}}\,d\eta; \quad A_2' = (\mu/\pi)A_2 \tag{17}$$
$$A_3 = \int_0^1 \frac{c}{R}\frac{\eta^4}{\sqrt{(\mu/\pi)^2+\eta^2}}\,d\eta; \quad A_3' = (\mu/\pi)A_3 \tag{18}$$

Aerodynamic forces and moments due to the engine at the engine assembly point on the wing are;

$$\begin{bmatrix} F_{x,Aero} \\ F_{y,Aero} \\ F_{z,Aero} \end{bmatrix}_{Eng(i)} = \begin{bmatrix} T_0 \\ F_{y,Hub} \\ F_{z,Hub} \end{bmatrix}_{Eng,Assembly} \tag{19}$$

$$\begin{bmatrix} M_{x,Aero} \\ M_{y,Aero} \\ M_{z,Aero} \end{bmatrix}_{Eng(i)} = \begin{bmatrix} 0 \\ -M_{y,Hub} + aRF_{z,Hub} \\ M_{z,Hub} + aRF_{y,Hub} \end{bmatrix}_{Eng,Assembly} \tag{20}$$

Inertial forces and moments due to the engine at the center of gravity point of aircraft are;

$$\begin{bmatrix} F_{x,Mass} \\ F_{y,Mass} \\ F_{z,Mass} \end{bmatrix}_{Eng(i)} = m_p \begin{bmatrix} \dot{u} \\ \dot{v} \\ \dot{w} \end{bmatrix} + m_p \begin{bmatrix} 0 & -\Delta z & \Delta y \\ \Delta z & 0 & -\Delta x \\ -\Delta y & \Delta x & 0 \end{bmatrix}_{Eng,AC} \begin{bmatrix} \dot{p} \\ \dot{q} + \dot{q}_p \\ \dot{r} + \dot{r}_p \end{bmatrix} \tag{21}$$

$$\begin{bmatrix} M_{x,Mass} \\ M_{y,Mass} \\ M_{z,Mass} \end{bmatrix}_{Eng(i)} = \begin{bmatrix} 0 & -\Delta z & \Delta y \\ \Delta z & 0 & -\Delta x \\ -\Delta y & \Delta x & 0 \end{bmatrix}_{Eng,AC} \begin{bmatrix} F_{x,Mass} \\ F_{y,Mass} \\ F_{z,Mass} \end{bmatrix}_{Eng(i)} + \begin{bmatrix} I_x & 0 & 0 \\ 0 & I_y & 0 \\ 0 & 0 & I_z \end{bmatrix}_{Eng(i)} \begin{bmatrix} \dot{p} \\ \dot{q} + \dot{q}_p \\ \dot{r} + \dot{r}_p \end{bmatrix} \tag{22}$$

The total forces and moments about the center of gravity point of aircraft due to one engine are,

$$\begin{bmatrix} F_{x,AC} \\ F_{y,AC} \\ F_{z,AC} \end{bmatrix}_{Eng(i)} = \begin{bmatrix} \cos(\psi)\cos(\theta) & -\sin(\psi) & \cos(\psi)\sin(\theta) \\ \sin(\psi)\cos(\theta) & \cos(\psi) & \sin(\psi)\sin(\theta) \\ -\sin(\theta) & 0 & \cos(\theta) \end{bmatrix} \begin{bmatrix} F_{x,Aero} \\ F_{y,Aero} \\ F_{z,Aero} \end{bmatrix}_{Eng(i)} + \begin{bmatrix} F_{x,Mass} \\ F_{y,Mass} \\ F_{z,Mass} \end{bmatrix}_{Eng(i)} \tag{23}$$

$$\begin{bmatrix} M_{x,AC} \\ M_{y,AC} \\ M_{z,AC} \end{bmatrix}_{Eng(i)} = \begin{bmatrix} 0 & -\Delta z & \Delta y \\ \Delta z & 0 & -\Delta x \\ -\Delta y & \Delta x & 0 \end{bmatrix}_{Eng,AC} \begin{bmatrix} F_{x,Aero} \\ F_{y,Aero} \\ F_{z,Aero} \end{bmatrix}_{Eng(i)} + \begin{bmatrix} M_{x,Aero} + M_{x,Mass} \\ M_{y,Aero} + M_{y,Mass} \\ M_{z,Aero} + M_{z,Mass} \end{bmatrix}_{Eng(i)} \tag{24}$$

Active Control Design

In this study, the primary objective was to achieve effective flutter control using the existing flight control surfaces, specifically the rudder and aileron. The control strategy employed in this study is based on a Proportional-Integral-Derivative (PID) controller. It is a well-established method in control systems engineering known for its simplicity and effectiveness in a wide range of applications. The PID-based control algorithm was integrated into the 6-DoF aircraft model developed in MATLAB & Simulink. The integration process involved the careful design and implementation of the control algorithm within the existing simulation environment, as illustrated in the Figure 1. The control gains for the PID controller were systematically tuned to achieve optimal performance.

The output of the PID controller is given by the following equation:

$$\delta_{Aileron,Cmd}(t) = K_{p,Aileron}\,\dot{\theta}_{Eng}(t) + K_{i,Aileron}\int_0^t \dot{\theta}_{Eng}(\tau)\,d\tau + K_{d,Aileron}\frac{d\dot{\theta}_{Eng}(t)}{dt} \tag{25}$$

$$\delta_{Rudder,Cmd}(t) = K_{p,Rudder}\,\dot{\psi}_{Eng}(t) + K_{i,Rudder}\int_0^t \dot{\psi}_{Eng}(\tau)\,d\tau + K_{d,Rudder}\frac{d\dot{\psi}_{Eng}(t)}{dt} \tag{26}$$

The combination of these three gains allows the PID controller to provide a robust and effective control strategy for a wide range of systems.

SIMULATION MODEL

The simulation model developed for this study integrates the classical Reed's whirl flutter framework into a 6-DoF aircraft model, focusing on the dynamics of propeller-driven aircraft. The model includes key aerodynamic and gyroscopic forces associated with the aircraft's propellers, which are critical to accurately capturing the onset of whirl flutter. By neglecting wing elasticity and concentrating on propeller aerodynamics, the model emphasizes the effects of gyroscopic interactions and the control system's role in suppressing instability. All these modelling studies were carried out as shown in Figures 2 and 3 using MATLAB-Simulink (Ref. 20), allowing for precise control over system dynamics and the implementation of control strategies. This approach enables an analysis of the aircraft's dynamic behaviour under various flight conditions.

The aircraft model utilized in this study is based on a single-jet-engine design with a validated simulation model. Based on the objective of this research, the propulsion subsystem was redesigned as shown in Figure 4. The updated model features a twin-engine configuration in which engines are mounted on

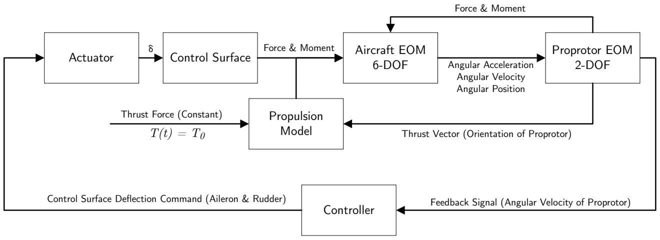

Figure 1. Block diagram of the control algorithm developed for active suppression of whirl flutter.

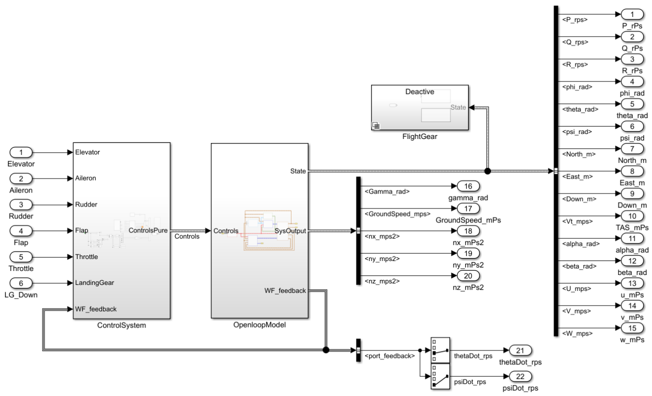

Figure 2. Overview of the simulation model.

the right and left wings. The twin engines are positioned slightly ahead of the aircraft's center of gravity, and aligned at the same level along the Z-axis. The parameters of the redesigned propulsion system in the simulation model are detailed in the Table 1, providing a comprehensive overview of the new configuration and its impact on the aircraft's aerodynamic behaviour. After the model development and control algorithm implementation, the simulation results indicated better performance with control applied to both aircraft pitch (θ) and yaw (ψ) axes.

Table 1. Parameters of the simulation model.

Name	Value	Description
m	12	Total mass (kg)
b	2.208	Wingspan (m)
$\bar{c}_w$	0.431	Mean aerodynamic chord of wing (m)
$\mathbf{r}_{AC}$	$[-1.06, 0, 0]$	Aircraft cg position wrt nose-tip (m)
$\mathbf{r}_{Eng}$	$[0.19, \pm 0.36, 0]$	Engine position wrt Aircraft cg (m)
Ω	840	Rotor angular velocity (rad/s)
N_B	2	Number of blades
R	0.2032	Rotor radius (m)
a	0.25	Pivot length to rotor radius ratio
I_x	1.03×10^{-4}	Rotor moment of inertia (kg m^2)
I_n	1.78×10^{-4}	Nacelle moment of inertia (kg m^2)
C_θ	0.015	Structural pitch damping (Nm s/rad)
C_ψ	0.015	Structural yaw damping (Nm rad^{-1})
K_θ	6	Structural pitch stiffness (Nm rad^{-1})
K_ψ	6	Structural yaw stiffness (Nm rad^{-1})
c_b	0.026	Blade chord (m)
cl_α	2π	Blade lift slope (rad^{-1})
ρ	1.225	Air density (kg/m^3)

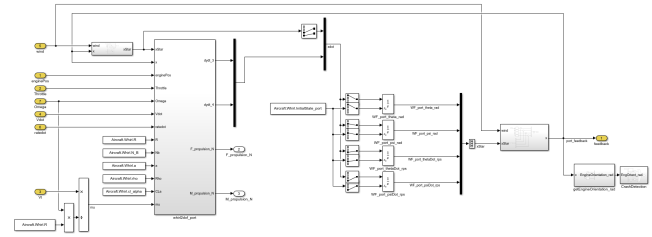

Figure 3. View of the proprotor engine subsystem.

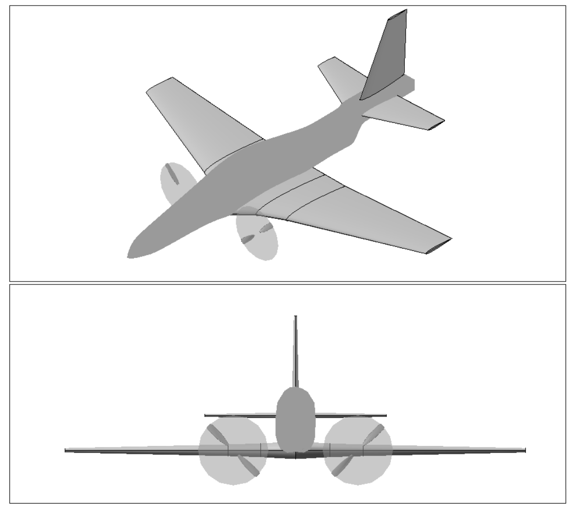

Figure 4. Isometric and front views of the aircraft used in the simulation study.

RESULTS AND DISCUSSION

The following section presents the results obtained from the numerical simulations, with the primary objective of assessing the effectiveness of the proposed control strategy in enhancing the system's stability and performance under various operating conditions. The numerical results are analyzed through key performance indicators such as system response and damping ratio, while comparative data from baseline scenarios, without control application, are provided to highlight the improvements achieved.

Given the need for high-frequency control surface commands to effectively suppress whirl flutter in a proprotor system, it was also crucial to ensure that actuator rate limits were not exceeded. Therefore, during the evaluation of the results from the simulations, it was examined whether the speeds of the control surface actuators exceeded the limits of the standard high-voltage servo motors (Ref. 21) typically used in similar aircraft.

At the start of the simulation, a 0.25-degree doublet was applied to the elevator with a step time of 0.1s, perturbing the system at velocities ranging from 50 m/s to 70 m/s. The upper left plot illustrates the time response of the engine pitch (θ), while the upper right plot shows the time response of the engine yaw (ψ). The lower left plot displays the aileron and rudder control surface deflections, and the lower right plot represents the corresponding actuator rates for both control surfaces.

Figure 5 shows that the system is naturally stable at lower velocities. Nevertheless, as velocity increases to 58.3 m/s, Figure 6 demonstrates that the open-loop system starts to approach marginal stability. Once the control system is activated, stability is achieved, confirming that the control system operates as expected.

In Figure 7, at 59 m/s, the oscillations in the open-loop system grow rapidly. When the control system is activated, stability is restored with a settling time of 1.3 seconds. Aileron deflections remain within ± 2 degrees, and rudder deflections within ± 0.5 degrees, with actuator rates below 100 deg/s. As seen in Figure 8, at 64 m/s, the settling time increases to 1.5 seconds, and actuator rates peak at 150 deg/s, which is still well below the allowable 460 deg/s limit.

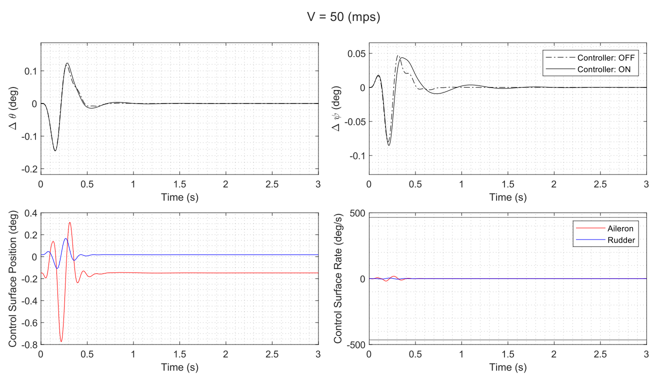

Figure 5. Engine pitch θ and yaw ψ response at 50 m/s.

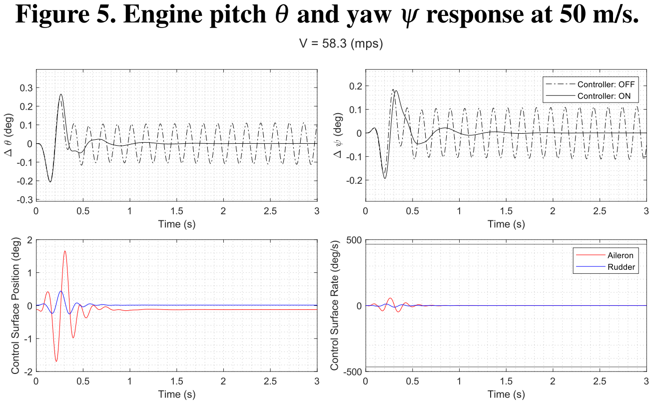

Figure 6. Engine pitch θ and yaw ψ response at 58.3 m/s

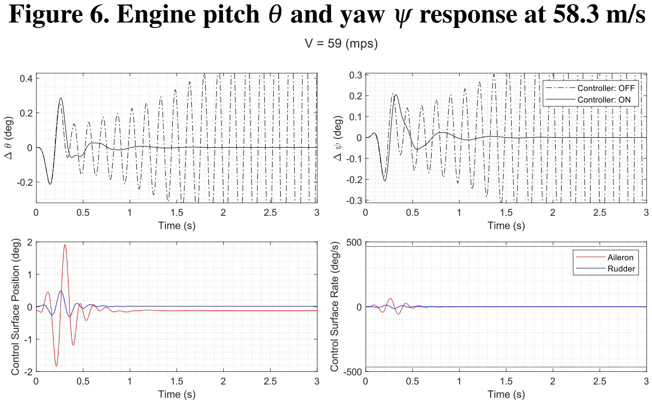

Figure 7. Engine pitch θ and yaw ψ response at 59 m/s

Figure 9 illustrates the system's behaviour at 66 m/s, where the control system significantly reduces oscillations, though it doesn't fully eliminate them. Aileron deflections reach up to 7.5 degrees and oscillate between ±2 degrees, while rudder deflections reach 1.5 degrees and oscillate between ±0.5 degrees. The required actuator rates peak at 210 deg/s but mostly remain below 100 deg/s. Finally, Figure 10 shows that at 66.8 m/s, the system with the active control system approaches marginal stability, with actuator rates reaching a maximum of 310 deg/s, which is still well below the 460 deg/s limit.

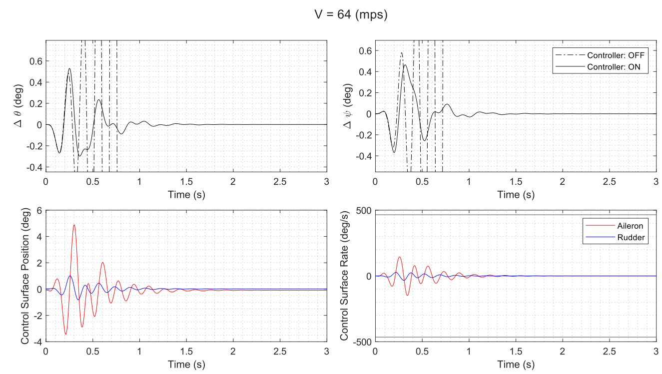

Figure 8. Engine pitch θ and yaw ψ response to at 64 m/s

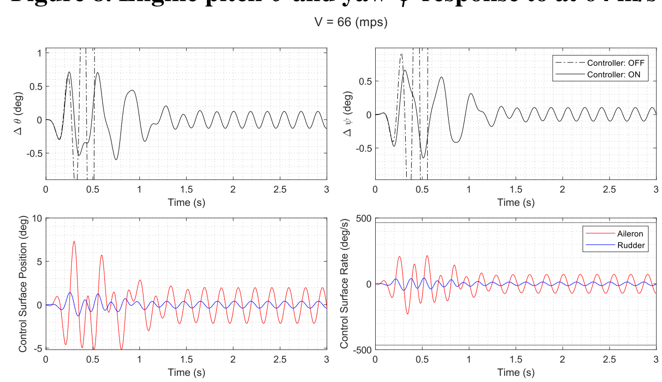

Figure 9. Engine pitch θ and yaw ψ response at 66 m/s

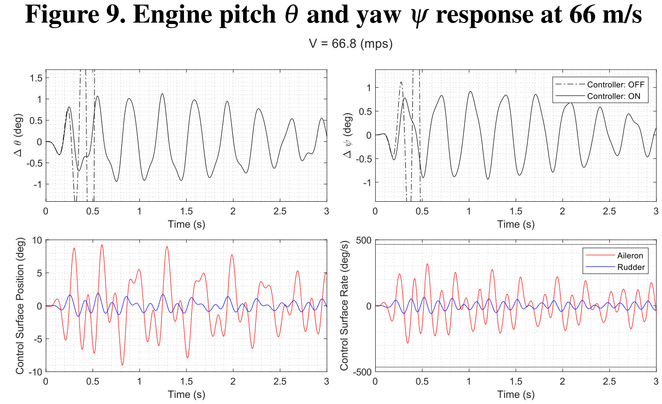

Figure 10. Engine pitch θ and yaw ψ response at 66.8 m/s

From the simulation outputs, the damping ratio was calculated using the *fminsearch* (Ref. 20) function, by applying a decreasing exponential method to the oscillation peaks. As shown in Figure 11, the stability boundary, which occurs at

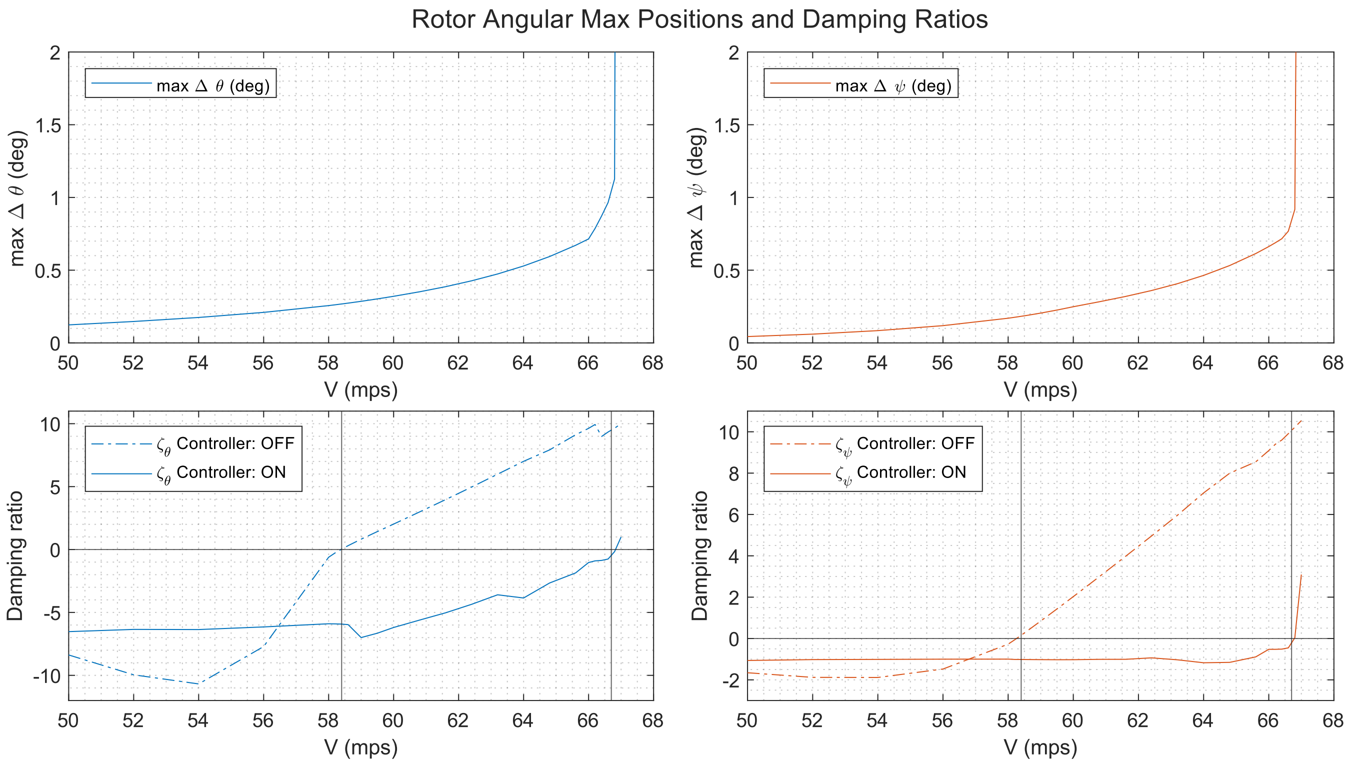

Figure 11. Illustrates the system's response characteristics including maximum angular displacements and corresponding damping ratios for pitch (θ) and yaw (ψ) axes.

58.3 m/s in the open-loop system, was increased to 66.8 m/s with the developed active control system.

In order to effectively suppress whirl flutter in a proprotor system operating at high frequencies, the actuator rate limit is crucial in the active control system design. The results indicate that the required control surface deflection rates remained below the specified limits. However, it is important to address potential issues such as backlash and low rate limits that may arise in the actuator. Examining these problems is essential to ensure the reliable performance of the control system.

CONCLUSIONS

Key findings from the study include:

- This study has investigated the usage of active control strategies to suppress whirl flutter in proprotor systems.
- Significant enhancements in the critical whirl flutter speed and overall aircraft stability were observed by integrating primary control surfaces such as the rudder and aileron into an active control system.
- The numerical simulations demonstrated a 14.6% increase in the critical whirl flutter speed, from 58.3 m/s to 66.8 m/s, highlighting the effectiveness of the proposed control approach.

Future work should focus on integrating wing aeroelastic effects and analyzing elevator deflections to develop more robust and efficient solutions for active whirl flutter suppression. Additionally, addressing potential actuator issues and further optimizing control strategies will be essential for improving system robustness and efficiency.

Author contact
Bedirhan Yilmaz: yilmazbe17@itu.edu.tr
Aykut Tamer: at2849@bath.ac.uk
Ali Tatar: tataral@itu.edu.tr

ACKNOWLEDGMENTS

Authors greatly acknowledge the travel support provided by Turkish Aerospace Industries to present this work.

REFERENCES

1. Frank T. Abbott, H. Neale Kelley, and Kenneth D. Hampton. Investigation of propeller-power-plant autoprecession boundaries for a dynamic-aeroelastic model of a four-engine turboprop transport airplane. Technical Note NASA-TN-D-1806, NASA, Langley Research Center Hampton, VA, USA, August 1963.
2. Wilmer H. Reed. Propeller-rotor whirl flutter: A state-of-the-art review. *Journal of Sound and Vibration*, 4(3):526–544, 1966.
3. Richard L. Bielawa. *Rotary Wing Structural Dynamics and Aeroelasticity*. AIAA, Washington, DC, 2nd edition, 2005.

4. Christopher Mair, Djamel Rezgui, and Branislav Titurus. Nonlinear stability analysis of whirl flutter in a rotor-nacelle system. *Nonlinear Dynamics*, 94:2013–2032, 2018. doi:10.1007/s11071-018-4472-y.

5. Anthony Quintana, Rui Vasconcellos, Glen Throneberry, and Abdessattar Abdelkefi. Nonlinear analysis and bifurcation characteristics of whirl flutter in unmanned aerial systems. *Drones*, 5(4), 2021.

6. Christopher Koch. Whirl flutter stability assessment using rotor transfer matrices. In *19th International Forum on Aeroelasticity and Structural Dynamics, IFASD 2022*, June 2022.

7. Aykut Tamer and Ali Tatar. A minimum complexity model for the aeroelastic analysis of distributed propulsion aircraft. In *49th European Rotorcraft Forum 2023 - Proceedings*, 09 2023.

8. Cecil W. Acree, Richard J. Peyran, and Wayne Johnson. Rotor design options for improving tiltrotor whirl-flutter stability margins. *Journal of the American Helicopter Society*, 46(2):87–95, April 2001. doi:10.4050/JAHS.46.87.

9. Eric Hathaway and Farhan Gandhi. Design optimization for improved tiltrotor whirl flutter stability. *Journal of the American Helicopter Society*, 52(2):79–89, April 2007. https://doi.org/10.4050/JAHS.52.79.

10. Sandilya Kambampati and Edward C. Smith. Aeroelastic optimization of high-speed tiltrotor wings with wing extensions and winglets. *Journal of Aircraft*, 54(5):1718–1727, 2017.

11. Haramura Bastos, Sérvio Túlio Suenai, and Rui Marcos Grombone de Vasconcellos. Whirl-flutter control through direct piezoelectric effect. *Engineering & Technology Scientific Journal*, 1(1), March 2023.

12. David Popelka, David Lindsay, and Donald J. Baker. Results of an aeroelastic tailoring study for a composite tiltrotor wing. In *American Helicopter Society 51st Annual Forum*, Fort Worth, TX, USA, May 9–11 1995.

13. Mark W. Nixon, David J. Piatak, Lawrance M. Corso, and David A. Popelka. Aeroelastic tailoring for stability augmentation and performance enhancements of tiltrotor aircraft. In *American Helicopter Society 55th Annual Forum*, Montreal, Canada, May 25–27 1999.

14. Lawrence M. Corso, David A. Popelka, and Mark W. Nixon. Design, analysis, and test of a composite tailored tiltrotor wing. *J. Am. Helicopter Society*, 45(3):207–215, July 2000. doi:10.4050/JAHS.45.207.

15. Ken-Ichi Nasu. Tilt-rotor flutter control in cruise flight. Technical Memorandum NASA-TM-88315, NASA, Ames Research Center, Moffett Field, CA, USA, December 1986.

16. Joerg P. Mueller, Yves Gourinat, Rogelio Ferrer, Tomasz Krysinski, and Benjamin Kerdreux. A numerical study on active control for tiltrotor whirl flutter stability augmentation. *Journal of the American Helicopter Society*, 51(3):244–254, July 2006. doi:10.4050/1.3092885.

17. Jinho Paik, Rupinder Singh, Farhan Gandhi, and Eric Hathaway. Active tiltrotor whirl-flutter stability augmentation using wing-flaperon and swash-plate actuation. *Journal of Aircraft*, 44(5):1439–1446, 2007.

18. Eric Hathaway and Farhan Gandhi. Tiltrotor whirl flutter alleviation using actively controlled wing flaperons. *AIAA Journal*, 44(11):2524–2534, 2006. doi:10.2514/1.18428.

19. Linghua Dong and Qiyu Li. Whirl flutter suppression of tiltrotor aircraft using actively controlled aileron. *Aerospace*, 9(12), 2022.

20. MATLAB. *9.9.0.2037887 (R2020b) Update 8*. The MathWorks Inc., Natick, Massachusetts, 2020.

21. Horizon Hobby, LLC. *Spektrum A6380 Standard High Voltage Metal Gear Servo Instruction Manual*.